

METALLICITIES FOR DOUBLE MODE RR LYRAE IN THE LARGE MAGELLANIC CLOUD ¹

A. Bragaglia¹, R.G. Gratton², E. Carretta², G. Clementini¹, L. Di Fabrizio¹, M. Marconi³

angela@bo.astro.it, gratton@pd.astro.it, carretta@pd.astro.it,
gisella@bo.astro.it, lau@bo.astro.it, marcella@na.astro.it

ABSTRACT

Metallicities for six double mode RR Lyrae's (RRd's) in the Large Magellanic Cloud have been estimated using the ΔS method. The derived $[\text{Fe}/\text{H}]$ values are in the range $[\text{Fe}/\text{H}] = -1.09$ to -1.78 (or -0.95 to -1.58 , adopting a different calibration of $[\text{Fe}/\text{H}]$ vs ΔS). Two stars in our sample are at the very metal rich limit of all RRd's for which metal abundance has been estimated, either by direct measure (for field objects) or on the basis of the hosting system (for objects in globular clusters or external galaxies).

These metal abundances, coupled with mass determinations from pulsational models and the Petersen diagram, are used to compare the mass-metallicity distribution of field and cluster RR Lyrae variables.

We find that field and cluster RRd's seem to follow the same mass-metallicity distribution, within the observational errors, strengthening the case for uniformity of properties between field and cluster variables

At odds to what is usually assumed, we find no significative difference in mass for RR Lyrae's in globular clusters of different metallicity and Oosterhoff types, or there may even be a difference contrary to the commonly accepted one, depending on the metallicity scale adopted to derive masses. This "unusual" result for the mass-metallicity relation is probably due, at least in part, to the inclusion of updated opacity tables in the computation of metal-dependent pulsation models.

Subject headings: Magellanic Clouds – stars: abundances – stars: oscillations – stars: variables: other (RR Lyrae) – techniques: spectroscopic

¹Osservatorio Astronomico di Bologna, Via Ranzani 1, 40127 Bologna, Italy

²Osservatorio Astronomico di Padova, Vicolo dell'Osservatorio 5, 35122 Padova, Italy

³Osservatorio Astronomico di Capodimonte, Via Moiariello 16, I-80131 Napoli, Italy

¹Based on observations collected at the European Southern Observatories, Chile

1. Introduction

The well-known dichotomy between *short* and *long* distance scales derived from old, population II stars has plagued astronomers for a long time and not even the impressive improvements in measuring distances due to the Hipparcos mission (see e.g., Gratton et al. 1997) seemed to provide an universally accepted solution. This is pointed out by the disagreement existing between results based on field or cluster stars. Methods founded on field stars, like statistical parallaxes or the Baade-Wesselink method applied to field RR Lyrae’s, or direct analysis of field horizontal branch stars (see Gratton 1998) seem to favour the *short* scale. Instead, cluster star-based distances, derived from main-sequence fitting to local subdwarfs (e.g. Gratton et al. 1997), or from pulsational properties of RR Lyrae’s in globular clusters (Sandage 1993), or from the calibration of the HB luminosity level using the Cepheid distance modulus of the LMC (Walker 1992), seem to support the *long* scale.

Following a calibration of the absolute magnitude of horizontal branch field metal-poor stars with good parallaxes from Hipparcos, Gratton (1998) suggested that a difference (at a ~ 0.1 – 0.2 mag level) might actually exist between the luminosity of HB stars in globular clusters (GC’s) and in the field. This result appeared to be confirmed by the difference in the average magnitude for field and cluster RR Lyrae’s in the LMC measured by Alcock et al. (1996) and Walker (1992) respectively (but see Clementini et al. 2001, hereafter C2001). Another indication in favour of this possible difference comes from the latest evolutionary models by Sweigart (1997), which include some extra-mixing of He and other heavy elements (C, N, O): as a matter of fact there is observational evidence for extra-mixing in cluster red giants but not among field stars (Gratton et al. 2000). On the other side, studies by Catelan (1998) and by Carretta, Gratton & Clementini (2000a) put this suggestion to a test using the pulsational properties of a selected sample of field and cluster RR Lyrae’s. Carretta et al. (2000a) show in a quantitative way that in our Galaxy, field and cluster RR Lyrae’s cannot be distinguished in a $\Delta \log P_{(\text{field-cluster})} - [\text{Fe}/\text{H}]$ plane: this goes towards excluding the possibility of a luminosity difference. In fact, the pulsational Period-Mass-Luminosity- T_{eff} relation (van Albada & Baker 1971) tells us that, at fixed T_{eff} , a difference in the period distribution (or its absence) indicates that there is (or there is not) a difference in the M/L ratio for the variables. The determination of star masses with the high precision required to settle the question is still one of the most difficult tasks in astrophysics. In this context double mode RR Lyrae’s are extremely powerful tools, because their masses can be estimated from the ratio of the two pulsational periods using pulsational models, hence independently from stellar evolution models. Unluckily, the $M - [\text{Fe}/\text{H}]$ relation can presently be studied in our Galaxy only using double mode pulsators in *clusters*, since only a handful of RRd’s have been so far identified in the *field* of our Galaxy.

The field RR Lyrae’s in the Large Magellanic Cloud bar play a key role in this respect, since i) projection effects are negligible, and they can be considered at the same distance from us and, ii) plenty of double pulsating variables have been identified in the field of the LMC by the MACHO experiment (Alcock et al. 1997, hereinafter A97). Field RR Lyrae’s in the LMC with good $[\text{Fe}/\text{H}]$ determinations may allow the derivation of both an accurate $L = f([\text{Fe}/\text{H}])$ (using single mode

pulsators) and a $M = f([\text{Fe}/\text{H}])$ relation, if any, (using double mode pulsators) within a homogeneous sample of field variables. The accuracy required to settle the question of the magnitude difference can be estimated from the pulsation equation of van Albada & Baker (1971), computed at fixed temperature and period: in order to appreciate a supposed difference of $\Delta \log L \sim 0.05$ (or 0.12 mag) we must detect a $\Delta \log M \sim 0.06$ (i.e. $\sim 0.12 M_{\odot}$) difference in mass between field and cluster variables. Cox (1991) using a fixed metallicity and the new OPAL (Rogers & Iglesias 1992) opacity tables found masses of $0.65 M_{\odot}$ for RR Lyrae pulsators in Oosterhoff type I clusters (Oo I; Oosterhoff 1939), and of 0.75 to even $0.85 M_{\odot}$ in Oosterhoff type II clusters (Oo II). Since the approximate difference in metallicity between the two Oo type clusters he studied is 0.5-0.7 dex, we estimate that an accuracy ≤ 0.2 dex in $[\text{Fe}/\text{H}]$ is then required.

We started an observational program on the field RR Lyrae’s of the LMC i) to derive their average apparent luminosity, and ii) to determine their metallicities (in particular for the RRd pulsators). The first part of the program, mostly dealing with new photometric data acquired by our team near the bar of the LMC, is described in C2001 and Di Fabrizio et al. (2001). The main results are the very accurate determination of the mean apparent magnitude of the field RR Lyrae’s of the LMC and the derivation of an independent reddening estimate.

From the light curves so derived we determined epochs to properly time the spectroscopic observations. In this paper we present metallicities with an accuracy of $\Delta [\text{Fe}/\text{H}] \sim 0.2$ dex for six RRd’s in the LMC. We used the ΔS index (Preston 1959), defined as $\Delta S = 10[\text{SpT}(\text{H}) - \text{SpT}(\text{K})]$, where $\text{SpT}(\text{H})$ and $\text{SpT}(\text{K})$ are the spectral types measured at minimum light, in units of tenths of a spectral type class, based on the hydrogen lines and on the CaII K line, respectively. In Section 2 we present the observational data and in Section 3 we describe the derivation of the ΔS values for the 6 stars. Section 4 is devoted to the determination of metallicities; in Section 5 we derive masses of our targets from the Petersen diagram, and discuss the mass-metallicity distribution. Summary and conclusions are presented in Section 6.

2. Observations and Reductions

The MACHO program discovered about 7,900 RR Lyrae’s in the twenty-two 40 arcmin^2 fields centered on the LMC bar (Alcock et al. 1996), and published coordinates and periods (but no epochs) for 73 RRd’s in the LMC bar (A97; differential light curves can be found in the MACHO website, e.g. wwwmcho.mcmaster.ca). Since the ΔS method requires the acquisition of spectra when variables are at minimum light, new photometric observations were obtained in order to derive complete ephemerides for some of A97 double mode pulsators. All observations were carried out in La Silla, Chile, in January 1999. Four nights at the Danish 1.54m telescope, one of which of photometric quality, were dedicated to Johnson V and B photometry (see C2001 for a complete description) and immediately reduced to produce light curves and derive ephemerides (epochs, in particular) for our targets. We tried to maximize the number of RRd’s observable in a single DFOSC (Danish Faint Object Spectrograph and Camera) pointing (field of view 13.5 arcmin^2),

and for the present program we selected 2 positions (in MACHO fields #6 and #13) comprising a total of 9 RRd’s; we refer to them as “field A” ($\alpha_{2000} = 05^h 22^m 44^s$ $\delta_{2000} = -70^\circ 34' 15''$) and “field B” ($\alpha_{2000} = 05^h 17^m 28^s$ $\delta_{2000} = -71^\circ 00' 14''$); henceforth RRd’s in the two fields will be indicated by CA or CB followed by an ordering number derived from tab. 1 of A97. Periods in A97 were used together with the epochs obtained from the new photometric data to properly schedule at minimum light the subsequent spectroscopic observations, done on 2 nights only 10 days afterwards. We did not use our own derived periods, since C2001 sampling of the light curve of the double mode pulsators (about 60 data-points in 4 consecutive nights) does not allow the derivation of periods for the RRd’s as accurate as in A97. We show in Figure 1 the light curve for one of the RRd’s based on C2001 data, and phased using A97 first overtone period P_1 . Finding charts for the 6 stars here discussed are presented in Figure 2, taken from C2001 photometry; maps are 200 arcsec², and the position of each RRd is indicated by a cross (not in scale), right at the center of the fields.

The spectroscopic observations were carried out at the 3.6m ESO telescope, during the nights 1999 January 17-18. EFOSC2 (ESO Faint Object Spectrograph and Camera) was used, mounting the CCD #40, a Loral $2k \times 2k$ chip, binned 2×2 , in combination with grism #7 (600 lines/mm, 3270-5240 Å) and a 1.5 arcsec wide slit, resulting in a $\simeq 9$ Å resolution (or $R \simeq 450$). Whenever possible, the slit was rotated in order to exclude nearby contaminating stars. Sky conditions were good enough for spectroscopic observations, but not of photometric quality, and the seeing varied from about 1” to 1.9”, with an average value around 1.5”.

We observed close to minimum light 7 of the 9 RRd’s within these fields, exploiting the previously described ephemerides, obtaining usable spectra for 6 of them (for one of the stars the spectrum is heavily contaminated by a very close bright object falling into the slit, and we excluded it). Identifications and information on these 6 targets are provided in Table 1. Equatorial coordinates come from the transformation of pixel positions to right ascension and declination, based on about one hundred stars individuated both in each of the two fields and on the Digitized Sky Survey⁵; they differ only a few arcsec from the ones published in A97. The $\langle V \rangle$ values are intensity averages and should be taken as preliminary, since a new calibration of the photometric data is under way (see C2001); epochs of maximum light are given in column 8. The fundamental and first overtone periods P_0 and P_1 are taken from A97. In column 9 and 10 we give the Heliocentric Julian Day of the spectroscopic observations of our targets and the corresponding phases computed using A97 first overtone pulsation periods and the epochs in column 8. Given the faintness of our targets ($V \simeq 19.5$ at minimum light), exposure times were in the range from 30 to 50 minutes, in order to reach the maximum possible S/N and avoid phase blurring on the pulsation cycle. Typical S/N ratios range from 10 to 30.

Thirteen non variable stars in the open cluster Collinder 140 (Cr 140, Clariá & Rosenzweig 1978, hereinafter CR), observed with the same instrumental configuration, were chosen as spectral

⁵The Digitized Sky Survey was produced at the Space Telescope Science Institute under U. S. Government grant NAG W-2166.

type standard stars, to apply the "classical" approach to the ΔS method via spectral types. The observed stars are indicated in Table 2, together with their Johnson B, V and Strömgren $b - y$ photometry, and spectral types derived both from CR, and from the Strömgren $b - y$ photometry (see next Section). The last column of the table gives the spectral type adopted in the present analysis: CR values or the average of CR types with those derived from the $b - y$, when both estimates are available.

For calibration purposes (i.e. to check that our ΔS 's are on the standard system) we took spectra at minimum light of 6 field ab type RR Lyrae's of known ΔS , namely IU Car, X Crt, WY Ant, AF Vel, U Lep and TV Leo; phases were derived from published ephemerides, and checked a posteriori by the spectral types (see note to Sect. 3.1). We also acquired 10 spectra along the pulsation cycle (from phase 0.0 to 0.65) of one c type RR Lyr (T Sex, also of known ΔS), in order to derive phase corrections for the spectra not exactly taken at minimum light.

Spectroscopic data were reduced using IRAF⁶ and the standard procedure for long slit spectra. Images were trimmed, bias subtracted, and flat-fielded; spectra were traced, extracted and wavelength calibrated. No flux-calibration was needed for our goals. We retained for further analysis only the wavelength range 3750–5210 Å, where all lines of interest are located. The most delicate parts of the whole procedure were spectrum extraction and background subtraction, since the observed fields are very crowded and the seeing conditions were not optimal. The risk of contamination from nearby objects is high; this happened, for instance, in the case of one of our targets. The background subtracted spectra of the 6 program stars are shown in Figure 3.

Spectral types were derived for our targets by comparing measured pseudo-equivalent widths (EW's) of $H\beta$, $H\gamma$, and of the Ca II K line with those measured in the stars of Cr 140. The pseudo-EW's were computed by dividing the instrumental fluxes within a small spectral region (f) centered on the selected feature, with the average of those in two comparison spectral regions (c_1 and c_2) located on both sides of each feature and defining the local continuum (see Table 3). All spectra were shifted to zero velocity before measuring the EW's. The (restframe) wavelength bins used are given in Table 3.

The spectral types for stars in Cr 140 given by CR are quite rough estimates. To reduce this source of error they were averaged, whenever possible, with the spectral types deduced from $uvby\beta$ colors (Hauck & Mermilliod 1998), using the calibrations by Crawford (1975, 1978, 1979). We then constructed curves calibrating EW's against spectral types using 13 of the 14 stars observed in Cr 140 (see Table 2 for identification); star #17 was excluded because it is not on the main sequence. Finally, we derived the best spectral type for each program spectrum by entering the measured EW's for the program star and reading out the corresponding spectral type. The final adopted H spectral type is the average of the values obtained from $H\gamma$ and $H\beta$. Following Preston (1959), the observed ΔS were simply the difference between the H and Ca II K spectral types, in tenths of

⁶IRAF is distributed by the NOAO, which are operated by AURA, under contract with NSF

spectral types. Results for the program stars are shown in Table 5, where we give for each of our targets the H and Ca spectral types, and the ΔS values derived applying both no phase corrections (as suggested by Kemper 1982), or using phase corrections deduced from T Sex (see Section 3.2). The corresponding metallicities are also presented in Table 5, and will be discussed in Sect. 4.

Our resolution is too coarse to separate the stellar and interstellar components of the Ca II lines, and we did not apply any correction for the contribution due to interstellar absorption, since its effect on the ΔS value, hence on $[\text{Fe}/\text{H}]$, is negligible. Gratton, Tornambè & Ortolani (1986), applying the ΔS method to the globular cluster ω Cen, employed a correction of 0.2 spectral subclasses (in the sense of an earlier spectral type) to their ΔS values, based on a reddening $E(B-V)=0.11$ mag. In our case the reddening is comparable (C2001), and the resulting correction would imply a difference in the derived $[\text{Fe}/\text{H}]$ of about 0.04 dex; this is negligible with respect to the total error associated to the method.

To estimate scale and random errors in our derived ΔS 's, we have compared the values we derived for the 6 comparison *ab*-type RR Lyrae's with those given in the literature (see Table 4 for individual values; the comparison is done between our values and the average of literature ΔS 's for each star). If we apply the phase corrections⁷ suggested by Butler (1975), our ΔS are on average smaller than the literature values by 0.2 ± 0.4 tenths of spectral types, with an *r.m.s.* of 1.2 tenths of spectral type for individual stars. Since the accuracy of the literature values is of the order of 0.5 tenths of spectral types, we conclude that our ΔS are on the standard scale, and have random errors of < 1 tenth of spectral type.

2.1. Phase Corrections

Before interpreting the observed ΔS in terms of metallicity, we have to apply a correction for the observed phase, since ΔS is known to vary during the pulsation cycle. The exact form of the phase-correction to be applied for *d*-type RR Lyrae's is not known. In their study of Galactic double pulsators in the field, Clement, Kinman & Suntzeff (1991) argued that the best correction is the same used for *c*-type RR Lyrae's, since in general the amplitude of the first harmonic is larger than the amplitude of the fundamental mode for double pulsators (this is also true for our program variables). Furthermore, the colors at minimum light of the *d*-type RR Lyrae's are much closer to those of the *c*-type at minimum than to the *ab*-type ones. Unfortunately, the phase corrections to ΔS for the *c*-type variables are not very well defined. Kemper (1982) studied the variation of

⁷All phases in col. 2 of Table 4 were inferred from the $\text{Sp}(\text{H})$'s of our spectra, and agree with those computed from literature ephemerides in all cases, but AF Vel and U Lep. These two stars have varying periods. Two ephemerides are available for AF Vel and the corresponding phases (0.58: Eggen 1994, and 0.63: Lub 1979) are slightly later than we derive; we suggest that both the ephemerides may be no longer adequate. Four ephemerides are available for U Lep (0.60: Firmanyuk, Derevyagin & Lysova 1985; 0.67: Lub 1979; 0.69: Eggen 1994; and 0.80: Fernley, Skillen & Burki 1983), and the phase we derive agrees with Eggen's prediction.

ΔS along the light curve of three *c*-type RR Lyrae's (RU Psc, T Sex, and DH Peg). He concluded that phase corrections are small (of the same order of the measuring error, i.e. ± 1 unit in ΔS) and should not be applied when the H spectral type is later than A7-A8, while he recommended to reject ΔS estimates from spectra where the derived H spectral type is earlier. An alternative procedure is to apply phase corrections to the ΔS according to the phase variation of ΔS derived from a well studied *c* type template star. We have used to this purpose our observations of T Sex, and derive (see Figure 4):

$$\Delta S_{\text{cor}} = \Delta S_{\text{obs}} + 0.587 [10.5 - SpT(H)],$$

where we give the correction simply as a linear function of the hydrogen spectral type and, according to Kemper (1982), we neglect the small difference existing between the ascending and descending part of the light curve. This seems a reasonable assumption for the *c*-type pulsators (but see Figure 1 of Smith 1986) given the fairly symmetrical shape of their light curves, which all show slow climbs to maximum light, and because spectra of RRc's do not seem to show the hydrogen line emissions and doubling which are the signature of shock waves propagating through the atmosphere, found in the spectra of the RRab's during the rise to maximum light (Preston & Paczyński 1964, Chadid & Gillet 1998, Gillet & Crowe 1998).

Using the above relationship, we obtain for T Sex $\Delta S = 6.81 \pm 0.09$ with an *r.m.s.* scatter of 0.26 tenths of spectral types. This value is to be compared with that determined using the procedure suggested by Kemper, that is $\Delta S = 6.28 \pm 0.17$ with an *r.m.s.* scatter of 0.50 tenths of spectral types. Also, for comparison the value given by Kemper for this star is $\Delta S = 6.1$ (6.3 if the star were analyzed as an *ab*-type variable). However, T Sex has the largest variation of ΔS with phase among the three stars considered by Kemper, so this procedure may lead to somewhat too large phase corrections (implying too large ΔS 's and too low metallicities). In Table 5 we give the ΔS values of our targets obtained using both the Kemper procedure (i.e. with no phase corrections and only using spectra later than A7-A8) and the phase corrections derived from T Sex light curve. On average, ΔS values corrected according to the T Sex curve are larger by 1.2 ± 0.2 spectral subtypes. Our adopted values are simply the average of those determined using the two different procedures. We estimate that uncertainties related to the phase correction are half the average difference between these two estimates, i.e. about 0.6 spectral subtypes.

3. Metallicities of the program stars

The ΔS values of our targets (both with and without phase corrections) were translated to metallicities using two different relations. The first one is given by Clementini et al. (1995, hereinafter C95), and is based on their study at high resolution and high S/N spectra of 10 field RRab's, on data adapted from Butler (1975) and Butler & Deming (1979), and on globular clusters having literature metallicities derived from high resolution spectra:

$$[\text{Fe}/\text{H}] = -0.194 \Delta S - 0.08. \quad (1)$$

The relation has been derived for *ab*-type RR Lyrae’s, however Kemper (1982) found that on average ΔS values derived for *ab* and *c*-type variables in GC’s agree with each other, so that also *d*-type RR Lyrae’s should obey approximately the same $\Delta S - [\text{Fe}/\text{H}]$ relation. Metallicities derived from this relation are quite similar to the Zinn & West (1984, hereafter ZW84) metallicity scale for GC’s.

The second one is given by Gratton (1999, hereafter G99), and recalibrates the ΔS index using the new metallicity scale for GC’s found by Carretta & Gratton (1997, hereafter CG97), which differs from ZW84’s especially at intermediate metallicities, usually giving somewhat higher metallicities. The metallicity dependence on ΔS is in this case

$$[\text{Fe}/\text{H}] = -0.176 \Delta S - 0.03, \quad (2)$$

which is only marginally consistent with the relation in C95. In the following we will be using metallicities derived from both relations:

(a) C95: ΔS values, both using no phase correction, as suggested by Kemper, and correcting using T Sex, are given in columns 4 and 5 of Table 5, and the adopted ΔS (the average of the two) is given in column 6. Columns 7 and 8 of Table 5 give the metallicities of the program stars computed using the ΔS estimates according to both Kemper procedure and T Sex phase corrections, respectively, adopting C95 relation. In the case of variable CA 48, we cannot give any metal abundance using Kemper procedure for the spectrum taken near maximum light, since the H-spectral type at which this star was observed is too early; the lower S/N spectrum, instead, can be used to determine ΔS values with both methods. Both spectra give similar results, and in the following we will be using the metallicity derived from the higher S/N spectrum. Column 9 contains the adopted metallicities on C95 scale: they are simply the average of the determinations obtained with the two different procedures. We estimate that internal uncertainties in these metallicities are of about ± 0.2 dex (from typical errors of ± 1 in our ΔS values). Systematic errors are mainly due to uncertainties in the phase corrections (± 0.1 dex) and in the metal abundance calibrations. The latter are however small (likely ± 0.1 dex) in the abundance range of interest for the program stars.

The average metal abundance of the program stars is $[\text{Fe}/\text{H}] = -1.46 \pm 0.09$ (5 stars, *r.m.s.* = 0.21 dex) when the Kemper procedure is used. A somewhat lower average value of $[\text{Fe}/\text{H}] = -1.60 \pm 0.13$ (6 stars, *r.m.s.* = 0.33 dex) is obtained when the phase corrections appropriate for T Sex are applied to the sample. Note that in the latter case we include in the average one more star (variable CA 48), which happens to be the most metal-rich of the sample. Finally, if we use the adopted $[\text{Fe}/\text{H}]$ ’s shown in col. 9, we obtain an average $[\text{Fe}/\text{H}] = -1.49 \pm 0.11$ (6 stars, *r.m.s.* = 0.28 dex). If we include the systematic errors present in our determinations, we conclude that, on C95 scale, our sample of 6 *d*-type RR Lyrae’s in the bar of the LMC has an average $[\text{Fe}/\text{H}] = -1.5 \pm 0.2$.

This compares rather well with the results obtained by Alcock et al. (1996). They used a similar method (line strengths of Ca II K and of H δ measured on medium-low resolution spectra of quite low S/N) and applied it to 15 field LMC RR Lyrae’s. Alcock et al. do not expand much on the subject: they do not give RR Lyr types, or individual values for metallicities. They only say that the most frequent [Fe/H] value is about -1.6 , with values in the range from -2.4 to -0.8 (see their fig. 8), and that the estimated accuracy is ± 0.25 dex.

(b) G99: Columns 10 and 11 of Table 5 contains the analogues of cols. 7 and 8, but using G99 relation, and col. 12 shows the adopted [Fe/H]’s, a simple mean of the two above. In this case the average values are [Fe/H]= -1.29 ± 0.07 (5 stars, *r.m.s.* = 0.16 dex) adopting Kemper procedure, [Fe/H]= -1.41 ± 0.12 (6 stars, *r.m.s.* = 0.30 dex) adopting phase corrections derived from T Sex, and [Fe/H]= -1.32 ± 0.10 (6 stars, *r.m.s.* = 0.25 dex) adopting the recommended values in col. 12. Again including systematic errors, we then conclude that, on G99 scale, our sample has a somewhat larger average metallicity, of [Fe/H]= -1.3 ± 0.2 .

The value compares slightly worse to Alcock et al. (1996), but this is not surprising, since CG97 scale tends to produce higher metallicities at this intermediate metal abundance. Anyway, 15 and 6 objects are too small samples to attach significance to a ~ 0.3 dex difference, well within the quoted uncertainties.

Notice that we have two RRd’s with [Fe/H] > -1.5 (C95) or > -1.3 (G99), hence with metal abundances larger than the Oo I clusters M 3 and IC 4499: these are the most metal-rich RRd’s identified so far.

4. Masses

4.1. The Petersen diagram

Masses for the double mode pulsators can be evaluated from the ratio between first overtone (P_1) and fundamental (P_0) pulsation periods. Petersen (1973) introduced the use of what is now universally known as ”the Petersen diagram”, where the ratio P_1/P_0 is plotted versus the value of P_0 for each RRd. Pulsation models define loci of constant mass in this diagram, hence RRd masses can be determined by the position of the star in the Petersen diagram, interpolating/extrapolating between these models.

Figure 5 shows the position in the Petersen diagram of the six LMC RRd’s studied in this paper (we have omitted from the figure the remaining 67 LMC RRd’s in A97 sample for clarity, but our small sample is well representative of the general P_1/P_0 versus P_0 distribution of the LMC RRd’s, see Figure 6), together with the other RRd’s found in our Galaxy (clusters and field) and in the Draco and Sculptor dwarf spheroidal galaxies. Data plotted in Figure 5 have been taken from Garcia-Melendo & Clement (1997) for NSV09295; from Clementini et al. (2000) for CU Com; from Clement et al. (1991, 1993) for AQ Leo, VIII-10, and VIII-58; from Clement et al. (1993)

for NGC 2419 (1 object), and NGC 6426 (1 object); from Corwin, Carney & Allen (1999) for M 3 (5 objects); from Walker & Nemeč (1996) for IC 4499 (17 RRd’s); from Walker (1994) for M 68 (12 RRd’s); from Nemeč (1985b) for M 15 (14 RRd’s); from Nemeč (1985a) for Draco (10 RRd’s); from Kaluzny et al. (1995) for Sculptor (1 object); from A97 for the LMC (73 RRd’s).

This figure is the analog of fig. 2 in A97; they also plotted the latest pulsational models available in literature, by Bono et al. (1996, henceforth BCCM96) computed for metallicity $Z=0.0001$, and for the three masses 0.65, 0.75 and 0.80 M_{\odot} . BCCM96 computed non-linear, non-local, time dependent pulsational models based on up-to-date opacities (Rogers & Iglesias 1992). These models, whose properties and physical and numerical assumptions are described in Bono & Stellingwerf (1994), in BCCM96 and in Bono et al. (1997a,b) are claimed by authors to reconcile values for masses and luminosities based on pulsation and on stellar evolution theories.

However, as already noted by A97, several objects (about 40 of the 73 double mode LMC RR Lyrae’s, among which our CA 02, and one of the RRd in M 3) fall in the region of the Petersen diagram below the 0.65 M_{\odot} BCCM96 model, and extrapolation of the BCCM96 models would produce rather small masses of about 0.55 M_{\odot} for these objects. This would not be simple to explain for the stars in this region with measured metallicity: M3 is the prototype Oosterhoff I cluster, and CA 02 and the Galactic field star VIII-58 have similar abundances, intermediate between Oo I and Oo II clusters ($[Fe/H] \simeq -1.7$ on C95 scale, or -1.5 on G99 scale). A97 discuss somewhat the problem, also suggesting, but in the end discarding, the possibility of these stars having a larger metal content, hence a mass larger than obtained by the BCCM96 models.

4.2. The pulsation models: derivation of the masses

Since we now have information on the metallicity of 6 LMC RRd’s, we have decided to test the dependence of masses derived from the Petersen diagram also on metallicity. In order to do this, we derive masses for all objects in Figure 5 for which the metallicity has been estimated, using the most appropriate models. Metallicities for all objects were adopted as follows: in the case of the LMC RRd’s we used the ΔS values (this paper), as for three MW field RRd’s (AQ Leo, VIII-10, VIII-58: Clement et al. 1991), and converted them to $[Fe/H]$ using both C95 and G99 relations; in the case of CU Com we used the $[Fe/H]$ value in Clementini et al. (2000), obtained from high resolution spectroscopy (note that at these low metal abundances ZW84 and CG97 scales coincide); for the dSph’s Draco and Sculptor we took the literature values (Mateo 1998) on ZW84 scale, and also converted them to CG97 scale according to the transformation relations provided by GC97 (see eq. 7 in that paper); for Galactic GC’s, since ΔS values were not available for all of them, we used the $[Fe/H]$ values available in the literature (ZW84 for all of them, CG97 direct measurements for M 3, M 15, M 68, and transformation to CG97 scale for NGC 2419, NGC 6426, and IC 4499). Metallicities chosen in the above way should be on a homogenous base for field and cluster variables, since the metallicity derived from the C95 relation (equation 1) is close to the ZW84 scale, while that derived from the G99 relation (equation 2) is close to the CG97 one.

Since both mass and metallicity affect the predicted Petersen diagram, information about the metallicity is required for a proper evaluation of the “pulsational” mass. At the same time, for each derived stellar mass the luminosity level can be inferred on the basis of the fundamental period range. We note that the only pulsation models that populate the Petersen diagram are those located in the double mode (OR) region of the predicted instability strip, that is between the theoretical fundamental blue edge and the theoretical first overtone red edge, for each assumed luminosity level. For each mass, models with different luminosity levels were computed in order to cover the full range of evolutionary predictions (which are dependent on the adopted input physics) for the luminosity of horizontal branch stars and also to take into account evolutionary effects (RR Lyrae evolving from their zero age horizontal branch location). As already noticed by BCCM96 nonlinear computations offer the opportunity to disentangle the mass and luminosity effects on the location in the Petersen diagram. As shown in Figure 5, once the mass and metallicity are fixed, the period values identify the luminosity level. However we consider the luminosity derivation beyond the aims of the present paper.

Models with $Z=0.0001$, 0.0004 , 0.0006 , 0.0008 have been computed for different masses and luminosities, using the same treatment as in BCCM96. In particular, we have used the following models: i) $Z = 0.0001$ at 0.85 , 0.83 , 0.80 , 0.75 , 0.65 , $0.63 M_{\odot}$ and with 3 luminosity levels, $\log L = 1.61$, 1.72 , 1.81 ; ii) $Z = 0.0004$ at 0.75 , 0.70 , 0.65 , 0.64 , 0.63 , 0.62 , $0.60 M_{\odot}$ and 3 luminosity levels, $\log L = 1.61$, 1.65 , 1.72 ; iii) $Z = 0.0006$ at 0.80 , 0.75 , $0.65 M_{\odot}$ and two luminosities, $\log L = 1.61$, 1.72 ; iv) $Z = 0.0008$ at 0.85 , $0.65 M_{\odot}$ and 3 luminosities, $\log L = 1.61$, 1.72 , 1.81 . A few additional models at $Z = 0.0002$, 0.001 , and 0.002 have also been computed, but not extensively used to determine masses. The main parameters of the adopted models (Z , mass, luminosity, P_0 , P_1) are given in Table 6, available only in electronic form.

A subset (indicated by a star symbol in Table 6) of the $Z=0.0001$, 0.0004 , 0.0006 and 0.0008 models is shown in Figure 5 where, for each metallicity, the upper curve refers to the higher mass, and the luminosity levels increase from right to left; now the models completely cover the range observed for the RRd’s. An enlargement of the region of interest for our 6 LMC RRd’s is shown in Figure 6, where all the LMC RRd’s from A97 are also plotted.

We derived masses for our targets as well as for all RRd’s for which a metal abundance estimate is available (either direct or of the hosting system) interpolating between the set of pulsational models at the four indicated metallicities. For each object we obtained a table with four mass values, one for each Z , and a fit with a parabola produced a quadratic relation mass *vs* Z . We then entered the empirical $[\text{Fe}/\text{H}]$ value for the star (we do it for both metallicity scales used in this paper) and derived the mass with the associated error (based on the error on the fit and an assumed 0.2 dex error on $[\text{Fe}/\text{H}]$). In some cases this procedure was slightly modified because the parabolic interpolation was not completely stable: for NGC 2419 and NGC 6426 we also used the $Z=0.0002$ models; for CU Com, the most metal-poor object of the sample, we found more adequate to use only the models at $Z=0.0001$, and similarly for CA 48 and CB 61 we used only the models at $Z=0.0008$, and for CB 49 only the models either at $Z=0.0006$ (on C95 scale) or at $Z=0.0008$

(on G99 scale). Results for masses and associated errors for the 6 LMC RRd’s, for the MW field RRd’s, and for the two dSph’s are given in Table 7, while Table 8 presents results for galactic clusters RRd’s.

Note that mass values for M 3 are the most uncertain because of the lower precision of the periods P_0 and P_1 given for its RRd’s. However, this could not be an explanation for the rather unusual masses found for the two Oo I clusters, since IC 4499 has exactly the same behaviour, but periods as precise as those of the other GC’s.

4.3. The mass-metallicity distribution

Figure 7 shows graphically these results; in panel (a) $[\text{Fe}/\text{H}]$ ’s are on C95 scale, and in panel (b) on G99 metallicity scale. The almost flat distribution of masses with varying metallicities, particularly in Figure 7(a), shows no indication of a mass - metallicity relation. In fact, mass and metallicity have an opposite effect on the position of a RRd in the Petersen diagram, leading to a sort of degeneracy. A mass - metallicity relation is only obtained using a fixed metallicity to compute the pulsational models, then using the derived masses in connection with the empirical abundances.

This is what was often done in the past (e.g., BCCM96, and fig. 1 in Cox 1991), but it implies neglecting the effect of the metal abundance on the position in the Petersen diagram, hence an error on the derived mass for all objects whose metallicities differ from the metal abundance adopted in the pulsational model computations. Petersen (1991), on the basis of linear calculations, found that the difference in metal abundance between Oo I and Oo II clusters produces a very small mass variation, whereas Cox (1991) predicts that the mass of all globular cluster RRd variables should be close to $0.8 M_{\odot}$ when metallicity is taken into account and the OPAL opacity tables for the proper composition are used. Our nonlinear computations show that the metallicity effect on the Petersen diagram is strong, since it acts in different ways on the fundamental and first overtone periods, and heavily influences their ratio. This result is in agreement with the predictions by Kovacs, Buchler & Marom (1991) and Cox (1995), who also found a noticeable dependence of the Petersen diagram on metallicity when the new OPAL opacities are used in pulsation computations. In particular Cox (1995) performs computations with $Z=0.0003$ and find a mass increase of OoI RRd with respect to those derived from models at $Z=0.0001$. However he reproduces the IC 4999 RRd’s location with $Z=0.0003$, $M=0.70 \pm 0.05 M_{\odot}$ models, whereas the metallicity used in our paper for IC 4999 RRd’s is equal or larger than 0.0006, depending on the metallicity scale. This most likely justifies the larger masses we find for OoI RRd’s with respect to Cox (1995) results. In fact, as shown in Figure 6, our $Z=0.0002-0.0004$, $M = 0.75 M_{\odot}$ models fit the IC 4999 RRd’s location too.

Further analysis on the metallicity dependence of pulsational models is required, since there is still the possibility that models could somehow overestimate the effect as a result of the adopted opacity tables (the most recent Livermore ones, Iglesias & Rogers 1996; see also the discussion by

Cox 1991) or that, as suggested by Kovacs et al. (1992) the Petersen diagram depends not only on the heavy element abundance, but also on the chemical mixture, but this issue is quite beyond the scope of the present paper.

In Figure 7(a), the globular clusters of both Oosterhoff groups have similar masses, with very similar internal scatter, while in Figure 7(b) the two Oo I clusters M3 and IC 4499 show a (unrealistically?) higher mass than the Oo II GC’s, as a result of the different (higher) metallicity scale adopted. Indeed, some weak hints of a mass metallicity relation with larger masses at higher metal abundances could be seen also among the Oo I field and cluster Rd’s in Figure 7(a). Whether this finding might imply an actual difference between GC’s, or is simply to impute to a too high sensitivity of the model-derived masses on metallicity, not well tuned yet, is an open question. The offset between the two metallicity scales is about 0.2 dex at the typical metallicity of the Oo I clusters; comparison between Figure 7(a) and Figure 7(b) tells quite clearly that a systematic error of 0.2 dex in the metallicity of the Oo I clusters, through the effect on the RRd’s masses derived from pulsational models, goes in the direction of producing a mass-metallicity relation (of any kind) that might actually not be there. The arrows in Figure 7 show graphically the variation of derived masses for a 0.2 dex increase in the assumed $[\text{Fe}/\text{H}]$, comparable to the error associated to abundances obtained with the ΔS method.

The derived masses are not in contrast to values expected from stellar evolutionary models for an age of 10-14 Gyr, and no extensive mass loss on the red giant branch. This is shown in Figure 7, where the lines represent the mass at the RGB tip for ages of 6, 8, 10, 12, and 14 Gyr; they are taken from the evolutionary models by Bertelli et al. (1994) for $Z=0.004$, 0.001, 0.0004, and by Girardi et al. (1996) for $Z=0.0001$, however any other choice of isochrone sets would produce similar results. Within the errorbars (see Tables 7, and 8) all objects in Figure 7(a) are well consistent with the plotted isochrone sets. Only the two most metal rich RRd’s of the LMC lie above the 10 Gyr isochrone; however, the large errorbar associated to their mass estimates on one hand, and/or the possibility for these field objects to be slightly younger than 10 Gyr might account for their position in the figure. Figure 7(b) is more difficult to explain, since RR’d in both M3 and IC4499 lie well above the 10 Gyr isochrone, even taking into account errorbars, and ages younger than 10 Gyr might be at the lower limit of the acceptable values for these GCs.

This could be due to uncertainty in the pulsational masses: models could have a too high sensitivity to abundances at these relatively large metallicities, either through the total heavy element abundance or the adopted chemical mixture. Another possibility is a too large abundance assumed for these clusters (e.g., an overestimate of about 0.15 dex in CG97 computations for intermediate-metallicity clusters). This last possibility can be checked for M 3, which has also been studied with high resolution spectroscopy and fine abundance analysis by Kraft et al. (1992); they find $[\text{Fe}/\text{H}]=-1.47 \pm 0.01$, to be compared to $[\text{Fe}/\text{H}]=-1.34 \pm 0.02$ in CG97. But also adopting the Kraft et al. value, the pulsational masses are larger than for the Oo II clusters. Furthermore, work on high resolution spectra of Turn Off stars in NGC 6752, obtained with UVES on the VLT (Gratton et al. 2001), obtains the same iron abundance already derived for giants in CG97 for this

intermediate metallicity cluster ($[Fe/H]=-1.42$). Small overestimates may be present, but do not seem to explain completely the effect noted in Figure 7(b). Finally, we wish to note that, based on a recent study of M 92 by King, Stephens & Boesgaard (1998), and on spectra of Turn Off stars in NGC 6397 (Gratton et al. 2001), it may be necessary to reassess also the low metallicity end of the GC scale, in the sense of lower abundances: this would go in the direction of increasing the metallicity difference between Oo I and Oo II clusters. Discussing the validity of metallicity scales is outside the scope of the present paper, and we prefer to derive masses using different ones, leaving to the reader the final choice about which one to believe better.

In any case, the major result here is that masses of Oo I and Oo II clusters do not significantly differ, or, if they do, they differ in the sense of Oo I GC's having higher masses, contrary to what usually accepted. This stems from the use of appropriate metallicities in the pulsational models. This result is summarized in Table 9 where we also compare the average mass values derived for the field and cluster variables of differing Oosterhoff types, adopting the two metallicity scales, separately. The cut between Oosterhoff types was set at $[Fe/H]=-1.7$ and -1.5 in ZW84 and CG97 respectively, with the Oo II variables being at $[Fe/H] \leq -1.7$ (-1.5).

The field RRd's have a larger scatter, both in metallicity and in mass; however most stars lie in the same region of the diagram occupied by the globular cluster stars. The bulk of the field Galactic RRd's as well as RRd's in Draco and Sculptor concentrate in the low metallicity region occupied by the Oo II clusters, while almost all of the LMC RRd's in our sample are in the region of the Oo I clusters, or extend further towards metallicity values which have no counterparts in our Galaxy or in the two dSph's where RRd's had been found in the past. This confirms C2001 finding that pulsational properties of the RR Lyrae variables in their observed regions of the LMC bar seem to follow the period-amplitude relation of Oo I clusters like M 3.

Finally note that, no matter which metallicity scale is adopted, cluster and field stars of similar metallicity and/or Oosterhoff type do not show any systematic difference in the derived mass.

5. Summary and conclusions

In order to investigate the possibility of a systematic difference in the mass and mass-metallicity distribution for RR Lyrae in globular clusters and in the general field, we have used the Preston ΔS method to derive metallicities for 6 RRd's (double pulsating variables) in the bar of the LMC. We have then combined these values with literature data for four field Galactic RRd's, making up a total of 10 field RRd's whose metallicity has been directly measured, and with data for RRd's in the Draco and Sculptor galaxies, for which the same metallicity as the host galaxy has been assumed. For these stars, pulsational masses were derived using an extension of the BCCM96 models to enlarged mass and metallicity ranges, purposefully computed for this paper. The same procedure has been applied to globular clusters RRd's, both of Oo I and Oo II types, similarly finding their masses.

We have then compared the position of field and cluster RRd's in the mass-metallicity diagram: we find that, on average, the two samples follow the same mass-metallicity distribution.

Since field and cluster RR Lyrae's also obey the same mass-luminosity-metallicity relation (Catelan 1998, Carretta et al. 2000a), we conclude that they should also obey the same luminosity-metallicity relation, and that there is no difference in luminosity between field and cluster RR Lyrae's. This result implies that results found for field RR Lyrae can be safely used also to derive properties of cluster RR Lyrae's, like e.g. the absolute luminosity and the absolute luminosity-metallicity relation.

We thank G. Bono for having provided data in tabular form and M. Tosi for very useful discussions on the mass-metallicity relation between Oosterhoff groups. We also wish to thank the anonymous referee for the suggested improvements which clarify our meaning. This research has made use of the Simbad database, operated at CDS, Strasbourg, France. This work was partially supported by MURST - Cofin98 under the project "Stellar Evolution."

REFERENCES

- Alcock, C. *et al.* (the MACHO collaboration) 1996, AJ, 111, 1146
- Alcock, C. *et al.* (the MACHO collaboration) 1997, ApJ, 482, 89 (A97)
- Bertelli, G., Bressan, A., Chiosi, C., Fagotto, F., & Nasi, E. 1994, A&AS, 106,275
- Bono, G., Caputo, F., Castellani, V., & Marconi M. 1996, ApJ, 471, L33 (BCCM96)
- Bono, G., & Stellingwerf, R.F. 1994, ApJS, 93, 233
- Bono, G., Caputo, F., Castellani, V., & Marconi M. 1997a, A&AS, 121, 327
- Bono, G., Caputo, F., Cassisi, S., Incerpi, R., Marconi, M. 1997b, ApJ, 483, 811
- Butler, D. 1975, ApJ, 200, 68
- Butler, D., & Deming, D., 1979, AJ, 84, 86
- Carretta, E., & Gratton R.G. 1997, A&AS, 121, 95 (CG97)
- Carretta, E., Gratton, R.G., & Clementini G. 2000a, MNRAS, 316, 721
- Catelan, M. 1998, ApJ, 495, L81
- Chadid, M., & Gillet, D. 1998, A&AS, 260, 123
- Clariá, J.J., & Rosenzweig, P. 1978, AJ, 83, 278, (CR)
- Clement, C.M., Kinman, T.D., & Suntzeff N.B. 1991, ApJ, 372, 273
- Clement, C.M., Ferance, S & Simon, N. 1993, ApJ, 412, 183
- Clementini, G., Carretta, E, Gratton, R.G., Merighi, R., Mould, J.R., & McCarthy, J.K. 1995, AJ, 110, 2319 (C95)
- Clementini, G., *et al.* 2000, AJ, 120, 2054
- Clementini, G., Gratton, R.G., Carretta, E., Bragaglia, A., Di Fabrizio, L., & Maio, M. 2001, AJ, submitted (C2001)
- Clube, S.V.M., Evans & Jones 1969, MemRAS, 72, 101
- Costar, D., & Smith, H.A. 1988, AJ, 96, 1925
- Corwin, T.M., Carney, B.W., & Allen, D.M. 1999, AJ, 117, 1332
- Cox, A.N. 1991, ApJ, 381, L71
- Cox, A.N. 1995, in Astrophysical applications of powerful new databases, S.J.Adelman, W.L.Wiese eds, Astronomical Society of the Pacific, p. 243
- Crawford, D.L., 1975, AJ, 80, 955
- Crawford, D.L., 1978, AJ, 83, 48
- Crawford, D.L., 1979, AJ, 84, 1858
- Di Fabrizio, L. Clementini, G., Gratton, R.G., Carretta, E., & Bragaglia, A. 2001, A&A, submitted

- Eggen, O.J. 1994, AJ, 107, 1834
- Fernley, J.A., Skillen, I., & Burki, G. 1993, A&AS, 97, 815
- Firmanyuk, B.N., Derevyagin, V.G., & Lysova, L.E. 1985, ATsir, 1374, 7
- Garcia-Melendo, E., & Clement, C.M. 1997, AJ, 114, 1190
- Gillet, D., & Crowe, R.A. 1998, A&A199, 242
- Girardi, L., Bressan, A., Chiosi, C., Bertelli, G., & Nasi, E. 1996, A&AS, 117, 113
- Gratton, R.G. 1998, MNRAS, 296, 739
- Gratton, R.G. 1999, in Globular Clusters, C.Martinez Roger, I.Pérez Fournón and F.Sánchez eds, Cambridge University Press, p. 155
- Gratton, R.G., *et al.* 2001, A&A, in press
- Gratton, R.G., Fusi Pecci, F., Carretta, E., Clementini, G., Corsi, C.E., & Lattanzi, M. 1997, ApJ, 491, 749
- Gratton, R.G., Sneden, C., Carretta, A., & Bragaglia, A. 2000, A&A, 354, 169
- Gratton, R.G., Tornambé, A., & Ortolani, S. 1986, A&A, 169, 111
- Hauck, B., & Mermilliod, M. 1998, A&AS, 129, 431
- Iglesias, C.A., & Rogers, F.J. 1996, ApJ, 464, 943
- Kaluzny, J., Kubiak, M., Szymanski, M., Udalski, A., Krzeminski, W., & Mateo, M. 1995, A&AS, 112, 407
- Kemper, E. 1982, AJ, 87, 1395
- King, J., Stephens A., & Boesgaard, A.M. 1998, AJ, 115, 666
- Kinman, T.D., & Carretta, E., 1992, PASP, 104, 111
- Kovacs, G., Buchler, R., Marom, A. 1991, A&A, 252, L27
- Kovacs, G., Buchler, R., Marom, A., Iglesias, C. A., Rogers, F. J., 1992, A&A, 259, L46
- Kraft, R.P., Sneden, C., Langer, G.E., & Prosser, C.F. 1992, AJ, 104, 645
- Lub, J., 1979, Ph.D. Thesis
- Mateo, M., 1998, ARA&A, 36, 435
- Mendes de Oliveira, C., & Smith, H.A., 1990, PASP, 102, 652
- Nemec, J.M. 1985a, AJ, 90, 204
- Nemec, J.M. 1985b, AJ, 90, 240
- Oosterhoff, P.Th., 1939, Observatory, 62, 104
- Petersen, J.O. 1973, A&A, 27, 89
- Petersen, J.O. 1991, A&A, 243, 426

- Preston, G.W. 1959, *ApJ*, 130, 507
- Preston, G.W., & Paczyinski, B. 1964, *ApJ*, 140, 181
- Rogers, F.J., & Iglesias, C.A. 1992, *ApJ*, 401, 361
- Sandage, A. 1993, *AJ*, 106, 703
- Smith, H.A. 1986, *PASP*, 98, 1317
- Smith, H.A., & Perkins, G.J. 1982, *ApJ*, 261, 576
- Suntzeff, N.B., Kinman, T.D., & Kraft, R.P., 1994, *ApJS*, 93, 271
- Sweigart, A. 1997, *ApJ*, 474, L23
- van Albada, T.S., & Baker, N. 1971, *ApJ*, 169, 311
- Walker, A.R. 1992, *ApJ*, 390, L81
- Walker, A.R. 1994, *AJ*, 108, 555
- Walker, A.R., & Nemec, J.M. 1996, *AJ*, 112, 2026
- Walker, A.R., & Terndrup, D.M., 1991, *ApJ*, 378, 119
- Zinn, R., & West, M.J. 1984, *ApJS*, 55, 45

Table 1: Information on the observed RRd’s

Name	Macho ID	α 2000	δ 2000	$\langle V \rangle$ mag	P_0 day	P_1/P_0	Epoch –2451100 day	HJD –2451100 day	φ
CA02 (23032)	13.6691.4052	5 21 34.1	–70 31 52.1	19.67	0.46087	0.74266	83.62317	97.79014	0.74
CB45 (7467)	13.6080.591	5 18 16.6	–70 55 17.6	19.01	0.48089	0.74394	83.81805	97.62984	0.72
CA48 (4420)	06.6811.651	5 22 45.2	–70 36 35.7	19.35	0.48336	0.74457	83.70869	97.74300 96.55699	0.03 * 0.58
CB49 (3347)	13.5836.525	5 16 27.0	–71 02 32.8	19.19	0.48406	0.74453	85.67901	97.54534	0.51
CB61 (4509)	13.5958.518	5 17 37.5	–71 00 26.3	19.49	0.49861	0.74467	84.73568	97.58639	0.77
CA67 (3155)	06.6810.428	5 22 35.9	–70 38 28.4	19.14	0.51159	0.74555	86.70999	96.73102	0.59

*Two spectra are available for CA 48. The one at HJD=51197.74300 was observed around maximum light, while that taken at HJD=51196.55699 ($\varphi=0.58$) is of low S/N. However, the phase corrected ΔS we derive from the spectrum at early phase (5.2) is in extremely good agreement with that derived from the low S/N spectrum (5.3; see column 6 of Table 5)

Table 2: Informations on the spectral type standard stars observed in Cr 140

No.	V	B–V	$b - y$	Sp.Type (CR)	Sp.Type ($b - y$)	Sp.Type (adopted)
6	7.12	-0.04		A0		A0
8	7.49	0.02		A2		A2
9	7.59	-0.09	-0.042	A0	B6.3	B8
15	8.59	-0.06	-0.020	A0	B9.3	A0
16	8.68	0.40		F2		F2
17 ¹	8.70	0.70	0.467	F5	G0.2	
19	8.83	-0.02	-0.017	A0	B9.7	A0
22	8.97	0.42		F2		F2
24	9.00	0.19		A3		A3
26	9.15	0.20	0.111	A2	A5.5	A4
29	9.28	0.14		A2		A2
32	9.34	0.02	-0.005	A0	A9.9	A0
38	9.57	0.22	0.140	A5	A7.5	A6
42	9.71	-0.07		A0		A0

¹This star was observed, but not used, since it is not on the main sequence

Table 3: Spectral regions used to compute the pseudo-EW's

Line	Blue Continuum	Line Region	Red Continuum
Ca II K	$c_1=3850-3870 \text{ \AA}$	$f=3925-3950 \text{ \AA}$	$c_2=3940-3960 \text{ \AA}$
H γ	$c_1=4220-4280 \text{ \AA}$	$f=4320-4360 \text{ \AA}$	$c_2=4420-4480 \text{ \AA}$
H β	$c_1=4680-4780 \text{ \AA}$	$f=4840-4890 \text{ \AA}$	$c_2=4950-5050 \text{ \AA}$

Table 4: Field *ab*-type RR Lyrae: comparison between literature and the newly derived ΔS values

Star	φ	ΔS liter.	Reference liter.	SpT(H)	SpT(K)	ΔS obs.	ΔS corr.
IU Car	0.80	9	(a)	F3.2	A5.2	8.0	8.2
X Crt	0.77	10,10.4	(a,d)	F3.2	A4.3	8.9	9.1
	0.83	10,10.4	(a,d)	F3.5	A4.7	8.8	8.8
WY Ant	0.68	6	(a)	F2.2	A4.8	7.4	8.2
AF Vel	0.55(0.58-0.63)	7	(a)	F0.9	A5.2	5.7	7.2
U Lep	0.69(0.60-0.80)	8,9,9.4,9.22	(a,b,c,e)	F2.6	A4.3	8.3	8.8
TV Leo	0.69	10,10,9.9,10.49,10.8	(a,b,c,e,f)	F1.7	A3.1	8.6	9.7

References. — (a) Lub (1979); (b) Preston (1959); (c) Butler (1975); (d) Kinman & Carretta (1992); (e) Suntzeff, Kinman & Kraft (1994); (f) Walker & Terndrup (1991)

Table 5: H and Ca spectral types (cols. 2 and 3), ΔS values, and corresponding metallicities for the program stars.

Star	SpT	SpT	ΔS	ΔS	ΔS	[Fe/H]	[Fe/H]	[Fe/H]	[Fe/H]	[Fe/H]	[Fe/H]
	(H)	(K)	Kem	T Sex	adopt.	Kem	T Sex	adopt.	Kem	T Sex	adopt.
						(Clementini et al. 1995)			(Gratton 1999)		
CA 02	F1.6	A3.6	8.0	9.1	8.6	-1.63	-1.85	-1.74	-1.44	-1.63	-1.54
CB 45	F1.9	A4.2	7.5	8.4	8.0	-1.54	-1.71	-1.62	-1.35	-1.51	-1.43
CA 48	A7.2	A5.7	1.5	5.2	5.2		-1.09	-1.09		-0.95	-0.95
	F2.2	A7.3	4.9	5.7	5.3	-1.03	-1.19	-1.11	-0.89	-1.03	-0.96
CB 49	F0.9	A4.3	6.6	8.1	7.4	-1.36	-1.65	-1.50	-1.19	-1.46	-1.33
CB 61	F2.7	A6.8	5.9	6.4	6.2	-1.14	-1.32	-1.23	-1.07	-1.16	-1.11
CA 67	F0.5	A2.6	7.9	9.7	8.8	-1.61	-1.96	-1.78	-1.42	-1.74	-1.58

Table 6: Main parameters of the adopted pulsation models: ONLY AVAILABLE IN ELECTRONIC FORM

Table 7: ΔS values, metal abundances on the two metallicity scales discussed in the text, and individual masses for field RRd’s. Metallicities for Sculptor and Draco are for the whole systems, not for individual RRd’s, and are given only once.

Star/cluster	ΔS	[Fe/H] C95	[Fe/H] G99	Mass (C95) M_{\odot}	Mass (G99) M_{\odot}	Reference (for ΔS)
LMC-CA 02	8.6	-1.74 ± 0.20	-1.54 ± 0.20	0.588 ± 0.077	0.691 ± 0.128	(a)
LMC-CB 45	8.0	-1.62 ± 0.20	-1.43 ± 0.20	0.742 ± 0.135	0.890 ± 0.195	(a)
LMC-CA 48	5.2	-1.09 ± 0.20	-0.95 ± 0.20	1.034 ± 0.240	1.034 ± 0.240	(a)
LMC-CB 49	7.4	-1.50 ± 0.20	-1.33 ± 0.20	0.860 ± 0.240	1.032 ± 0.240	(a)
LMC-CB 61	6.2	-1.23 ± 0.20	-1.11 ± 0.20	1.075 ± 0.250	1.075 ± 0.250	(a)
LMC-CA 67	8.8	-1.78 ± 0.20	-1.58 ± 0.20	0.765 ± 0.102	0.928 ± 0.196	(a)
MW-CU Com	–	-2.38 ± 0.20	-2.38 ± 0.20	0.835 ± 0.120	0.835 ± 0.120	(b)
MW-VIII-10	9.2	-1.86 ± 0.20	-1.66 ± 0.20	0.708 ± 0.063	0.812 ± 0.143	(c)
MW-VIII-58	8.6	-1.75 ± 0.20	-1.55 ± 0.20	0.605 ± 0.075	0.722 ± 0.138	(c)
MW-AQ Leo	8.9	-1.81 ± 0.20	-1.60 ± 0.20	0.831 ± 0.098	0.987 ± 0.199	(d,c)
Draco-V11	–	-2.0 ± 0.15	-1.83 ± 0.15	0.758 ± 0.042	0.786 ± 0.054	
Draco-V72	–			0.763 ± 0.008	0.801 ± 0.085	
Draco-V83	–			0.759 ± 0.008	0.798 ± 0.086	
Draco-V112	–			0.810 ± 0.008	0.849 ± 0.088	
Draco-V138	–			0.760 ± 0.008	0.798 ± 0.084	
Draco-V143	–			0.783 ± 0.007	0.824 ± 0.091	
Draco-V156	–			0.744 ± 0.008	0.781 ± 0.080	
Draco-V165	–			0.634 ± 0.009	0.667 ± 0.071	
Draco-V169	–			0.757 ± 0.008	0.795 ± 0.085	
Draco-V190	–			0.751 ± 0.008	0.789 ± 0.085	
Sculptor-V1168	–	-1.8 ± 0.10	-1.58 ± 0.15	0.782 ± 0.092	0.934 ± 0.185	

References. — (a) This paper; (b) Clementini et al (2000a); (c) Clement et al. (1991); (d) Mendes De Oliveira & Smith (1990)

Table 8: ΔS values, masses and metal abundances for the cluster RRd's. Metallicities are for the whole systems, not for individual RRd's, and are given only once per cluster. ¹

Star/cluster	ΔS	[Fe/H] ZW84	[Fe/H] CG97	Mass (C95) M_{\odot}	Mass (G99) M_{\odot}	Reference (for ΔS)
NGC 6426 - V3	–	-2.20 ± 0.20	-2.11 ± 0.20	0.814 ± 0.039	0.803 ± 0.012	
M 15 - V17	11.3	-2.15 ± 0.20	-2.12 ± 0.06	0.849 ± 0.072	0.839 ± 0.056	(a)
M 15 - V26	11.3			0.789 ± 0.067	0.780 ± 0.052	(a)
M 15 - V30	11.3			0.776 ± 0.063	0.767 ± 0.048	(a)
M 15 - V31	11.3			0.797 ± 0.067	0.787 ± 0.052	(a)
M 15 - V39	11.3			0.790 ± 0.072	0.780 ± 0.056	(a)
M 15 - V51	11.3			0.700 ± 0.048	0.693 ± 0.036	(a)
M 15 - V53	11.3			0.803 ± 0.066	0.793 ± 0.051	(a)
M 15 - V58	11.3			0.795 ± 0.067	0.786 ± 0.052	(a)
M 15 - V61	11.3			0.758 ± 0.061	0.750 ± 0.047	(a)
M 15 - V67	11.3			0.787 ± 0.066	0.777 ± 0.051	(a)
M 15 - V96	11.3			0.790 ± 0.070	0.781 ± 0.054	(a)
NGC 2419 - V39	–	-2.10 ± 0.20	-1.97 ± 0.20	0.793 ± 0.009	0.801 ± 0.030	
M 68 - V7	10.8	-2.09 ± 0.20	-1.99 ± 0.06	0.777 ± 0.042	0.769 ± 0.011	(a)
M 68 - V8	10.8			0.761 ± 0.039	0.754 ± 0.012	(a)
M 68 - V3	10.8			0.759 ± 0.038	0.752 ± 0.012	(a)
M 68 - V45	10.8			0.746 ± 0.036	0.740 ± 0.012	(a)
M 68 - V19	10.8			0.771 ± 0.040	0.764 ± 0.011	(a)
M 68 - V29	10.8			0.768 ± 0.039	0.761 ± 0.012	(a)
M 68 - V4	10.8			0.757 ± 0.037	0.750 ± 0.012	(a)
M 68 - V31	10.8			0.765 ± 0.037	0.758 ± 0.012	(a)
M 68 - V34	10.8			0.740 ± 0.033	0.735 ± 0.012	(a)
M 68 - V21	10.8			0.772 ± 0.037	0.765 ± 0.012	(a)
M 68 - V26	10.8			0.725 ± 0.029	0.721 ± 0.012	(a)
M 68 - V36	10.8			0.717 ± 0.027	0.713 ± 0.013	(a)

Table 8: (continued)

Star/cluster	ΔS	[Fe/H] ZW84	[Fe/H] CG97	Mass (C95) M_{\odot}	Mass (G99) M_{\odot}	Reference (for ΔS)
M 3 - V68	8.4	-1.66 ± 0.20	-1.34 ± 0.06	0.677 ± 0.108	0.930 ± 0.204	(a)
M 3 - V79	8.4			0.772 ± 0.140	1.106 ± 0.270	(a)
M 3 - V87	8.4			0.795 ± 0.148	1.147 ± 0.286	(a)
M 3 - V99	8.4			0.846 ± 0.164	1.239 ± 0.318	(a)
M 3 - V166	8.4			0.803 ± 0.150	1.160 ± 0.289	(a)
IC 4499 - V78	6.9	-1.50 ± 0.20	-1.26 ± 0.20	0.841 ± 0.181	1.116 ± 0.267	(b)
IC 4499 - V18	6.9			0.830 ± 0.177	1.100 ± 0.260	(b)
IC 4499 - V65	6.9			0.832 ± 0.177	1.101 ± 0.261	(b)
IC 4499 - V10	6.9			0.827 ± 0.175	1.093 ± 0.257	(b)
IC 4499 - V21	6.9			0.833 ± 0.177	1.103 ± 0.261	(b)
IC 4499 - V51	6.9			0.844 ± 0.180	1.118 ± 0.266	(b)
IC 4499 - V109	6.9			0.850 ± 0.183	1.128 ± 0.269	(b)
IC 4499 - V59	6.9			0.849 ± 0.181	1.125 ± 0.267	(b)
IC 4499 - V87	6.9			0.856 ± 0.184	1.135 ± 0.271	(b)
IC 4499 - V63	6.9			0.838 ± 0.177	1.107 ± 0.260	(b)
IC 4499 - V73	6.9			0.854 ± 0.182	1.130 ± 0.268	(b)
IC 4499 - V42	6.9			0.901 ± 0.199	1.204 ± 0.294	(b)
IC 4499 - V31	6.9			0.855 ± 0.181	1.130 ± 0.267	(b)
IC 4499 - V90	6.9			0.865 ± 0.184	1.144 ± 0.271	(b)
IC 4499 - V8	6.9			0.887 ± 0.190	1.176 ± 0.281	(b)
IC 4499 - V71	6.9			0.892 ± 0.191	1.182 ± 0.282	(b)

¹14 RRd's have been detected in M15, but 3 were not used because their periods were given as uncertain. IC4499 contains 17 RRd's, but periods are available only for 16 of them.

References. — (a) Costar & Smith (1988); (b) Smith & Perkins (1992)

Table 9: Mean masses for cluster and field RRd's.

	$\langle M \rangle_{GC}$	$\langle M \rangle_{field}$
ZW84		
[Fe/H] ≤ -1.7	0.772 ($\sigma=0.032$)	0.744 ($\sigma=0.072$)
[Fe/H] > -1.7	0.835 ($\sigma=0.048$)	0.928 ($\sigma=0.155$)
CG97		
[Fe/H] ≤ -1.5	0.765 ($\sigma=0.031$)	0.814 ($\sigma=0.082$)
[Fe/H] > -1.5	1.127 ($\sigma=0.059$)	1.008 ($\sigma=0.081$)

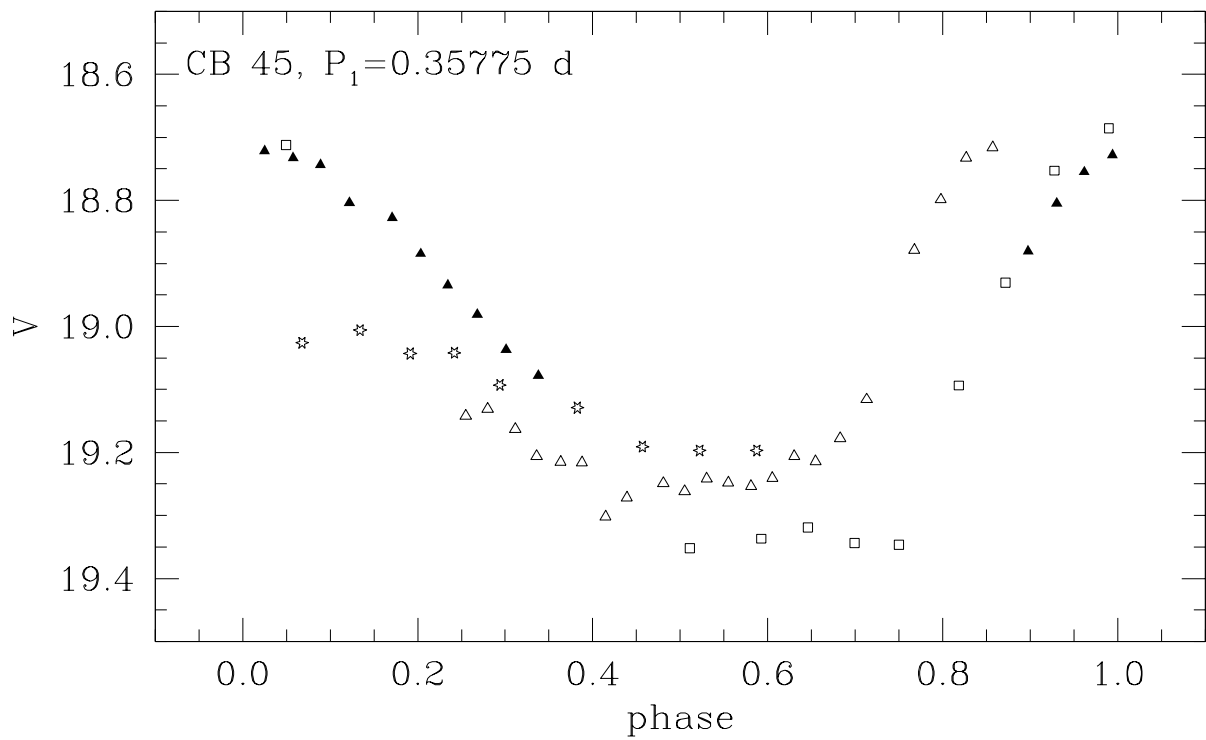


Fig. 1.— The LMC RRd CB 45: V light curve derived from C2000 photometry; the different symbols refer to the 4 different nights of observation. Data have been phased according to the first overtone period of pulsation (P_1) given in A97 and the epoch derived by C2000.

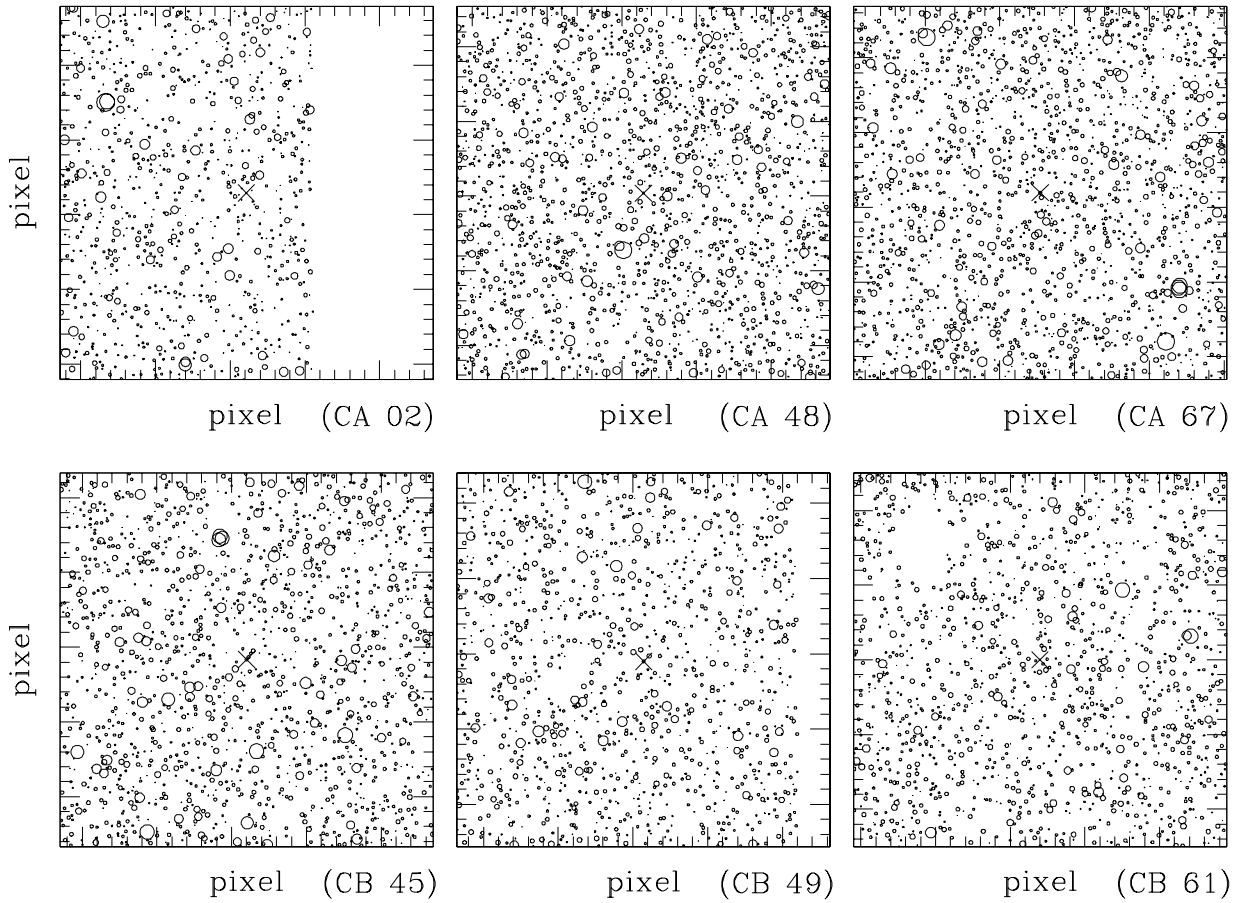


Fig. 2.— Finding charts for the 6 program stars derived from C2000 photometry (at top, from left to right: CA 02, CA 48, CA 67; at bottom, from left to right: CB 45, CB 49, CB 61). Each RRd is at the center, indicated by the cross (coordinates are found in Table 1); the fields shown cover 200 arcsec^2 , with North at top and East on the left.

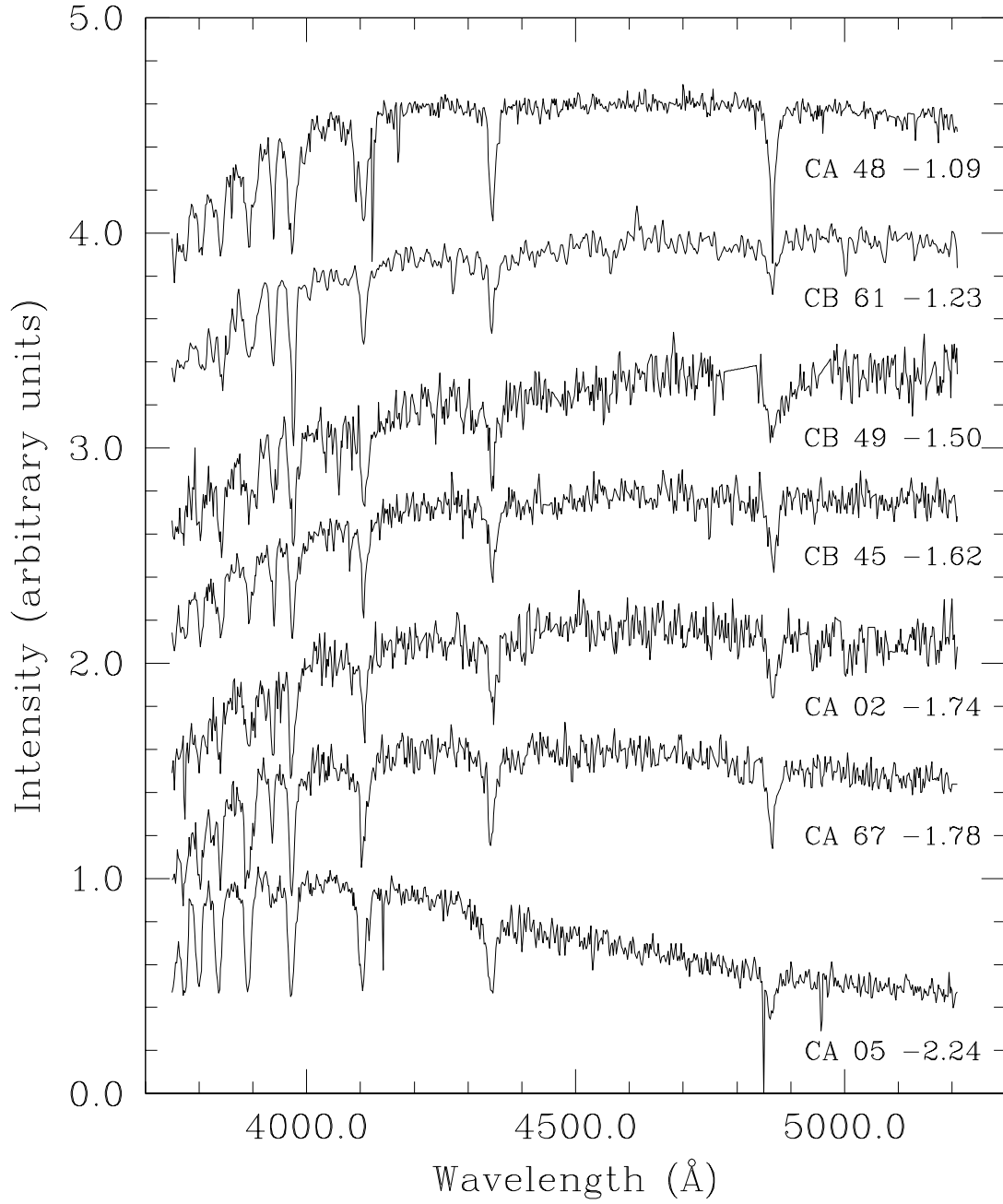


Fig. 3.— Spectra of the 6 program stars on an arbitrary intensity scale. They are shown in order of decreasing metallicity from top to bottom.

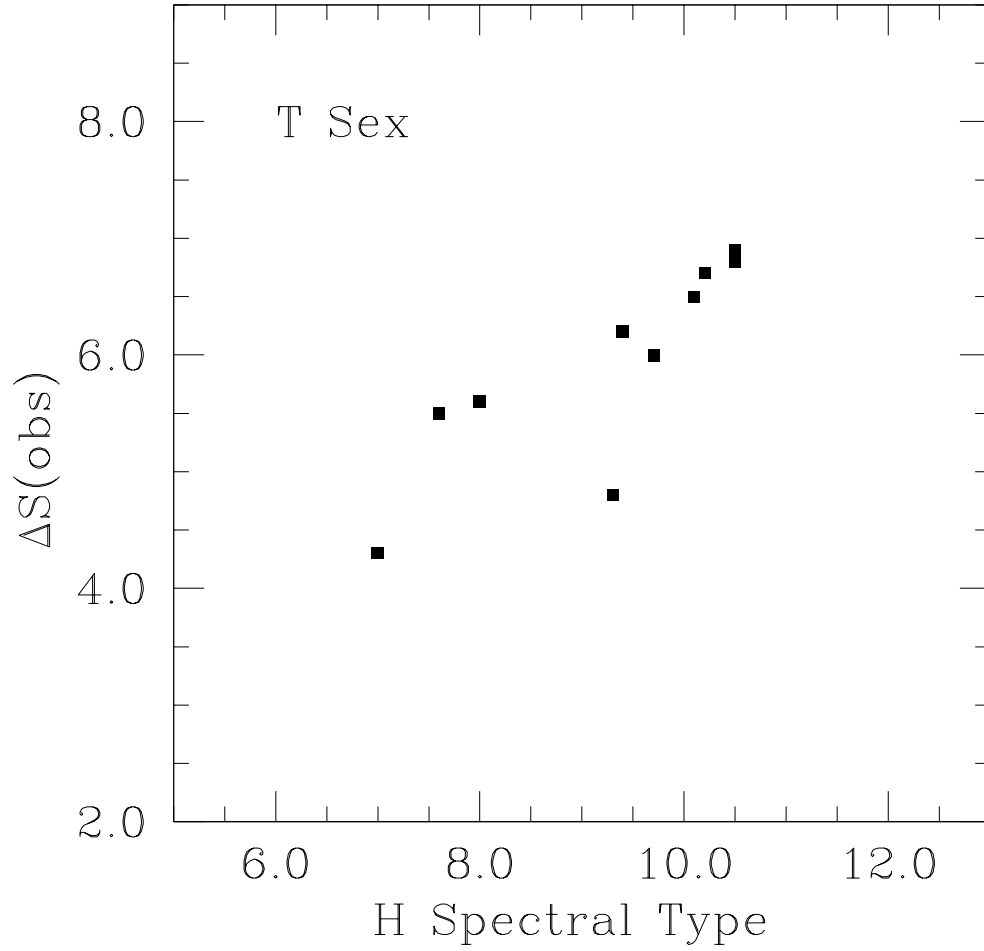


Fig. 4.— T Sex: variation of SpT(H) and of the corresponding ΔS for the 10 spectra from which we have derived the phase corrections described in Section 3.2.

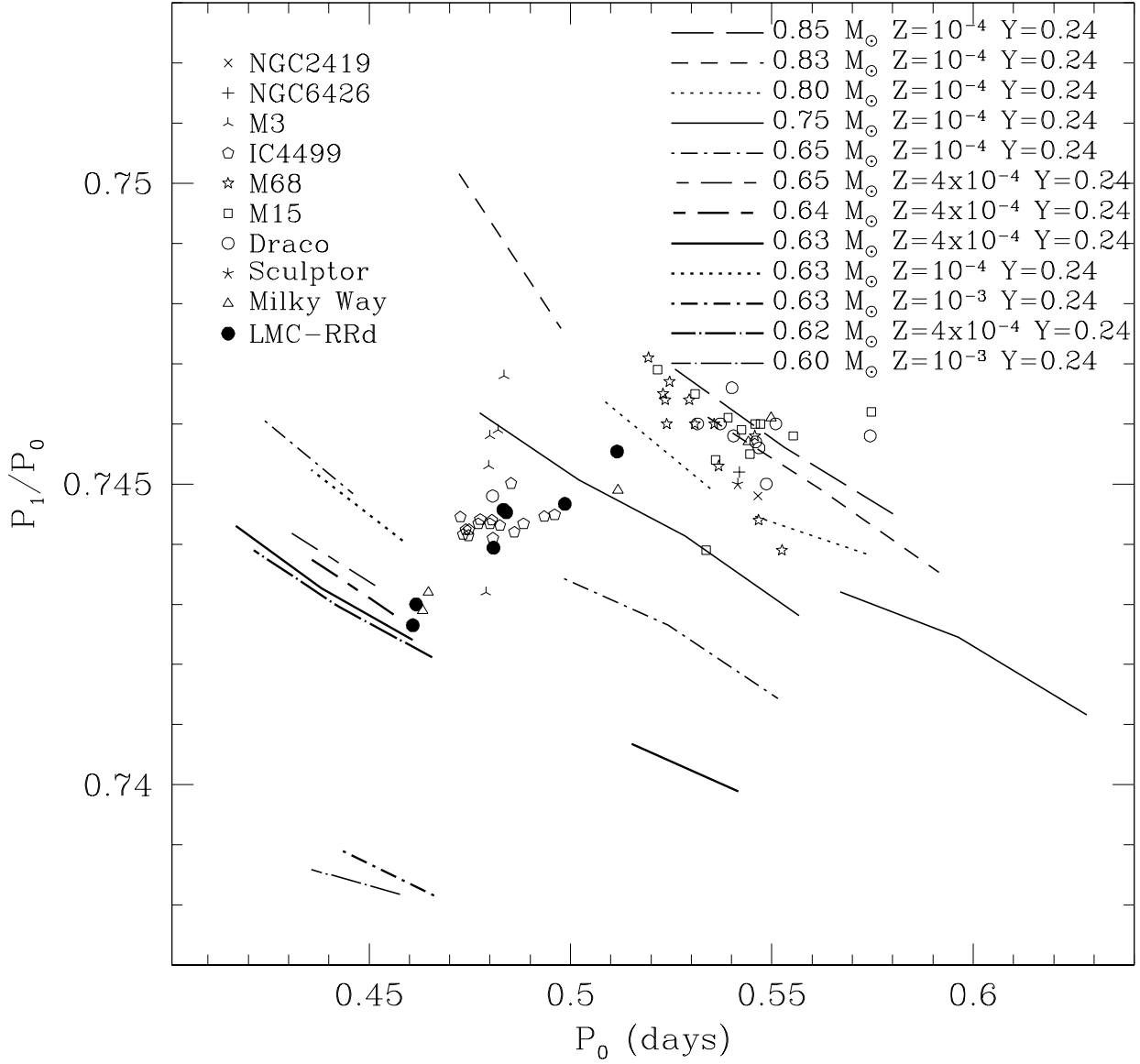


Fig. 5.— The Petersen diagram for known RRd’s in our Galaxy (both in the field and in globular clusters), in the two dwarf spheroidals Draco and Sculptor, and in the LMC, indicated by different symbols. Also plotted are the BCCM96 models ($Z = 0.0001$, and masses 0.80, 0.75, and 0.65 M_{\odot}) and some of the new models extending them to different metallicities and masses (See Section 5 for an explanation).

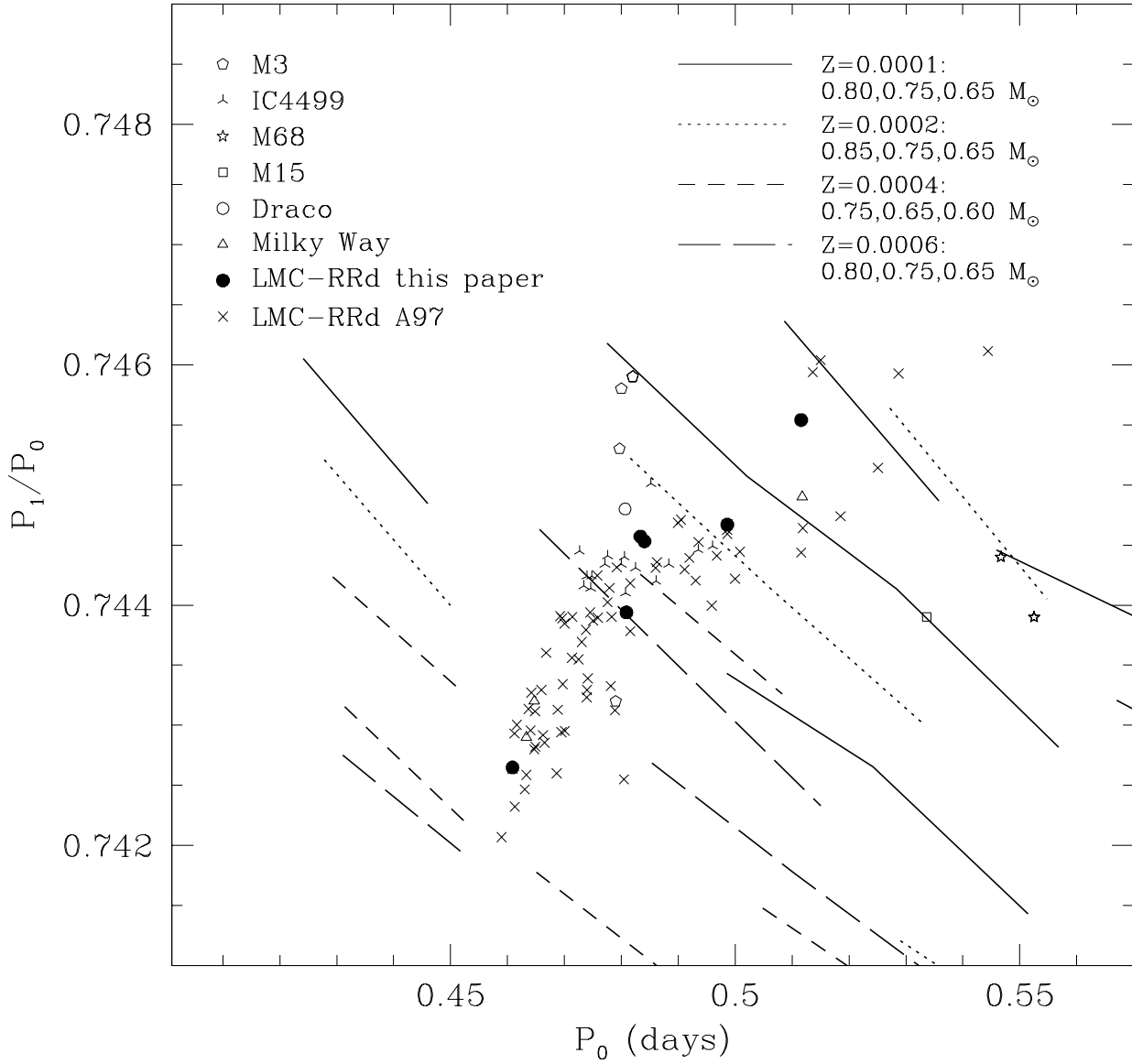


Fig. 6.— Enlargement of Figure 5 in the region relevant for LMC RRd's: here all LMC RRd's found by A97 are plotted.

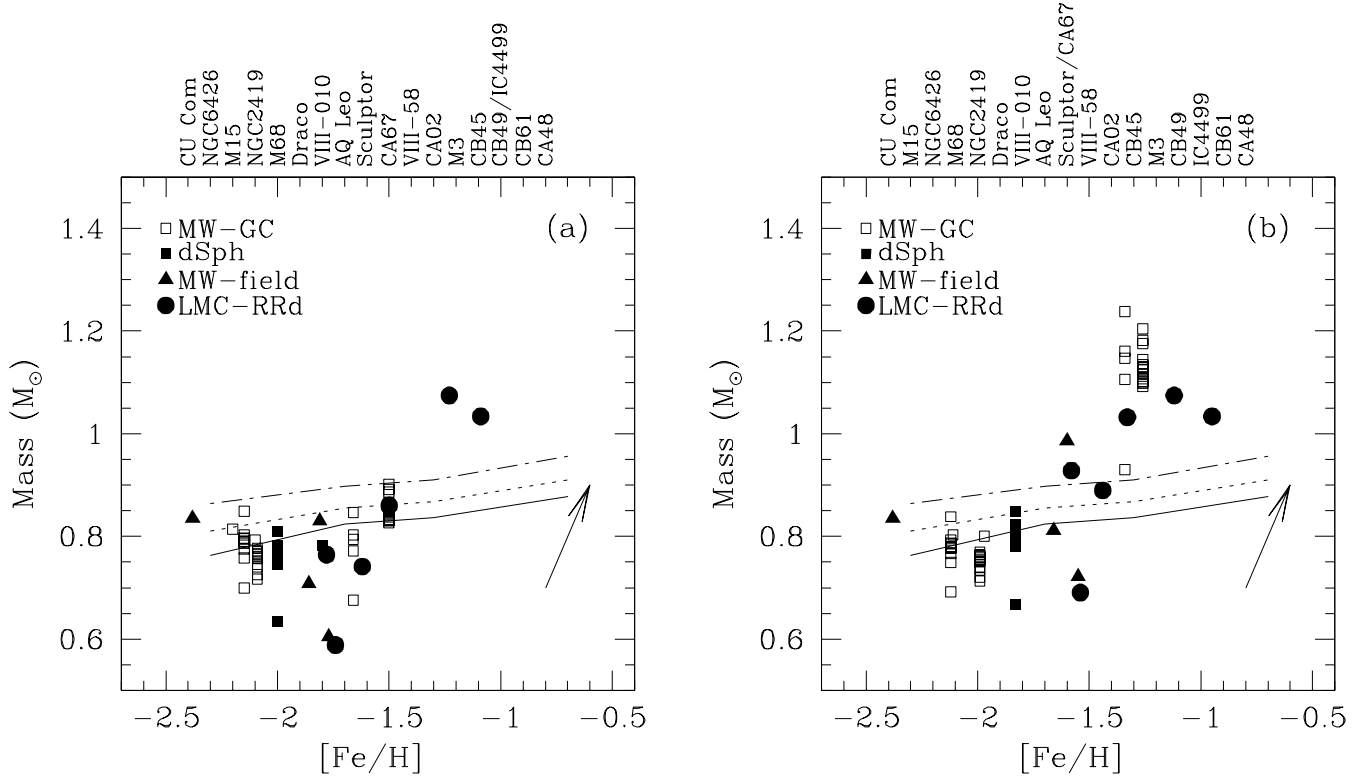


Fig. 7.— Mass - metallicity plots: (a) using metallicities on the ZW84 scale for GC’s and dSph’s, and C95 relation for RR Lyrae’s; (b) using metallicities on CG97 scale for GC’s and dSph’s, and G99 relation for RR Lyrae’s. See discussion in Section 5.3 for extensive comments on the high mass of the Oo I clusters. In both panels the program stars are indicated by filled circles, field RRd’s in our Galaxy by filled triangles, RRd’s in GC’s by open squares, and dSph’s by filled squares. References for the original papers are given in Section 5. Lines indicate the variation of mass at the RGB tip with metallicity, for ages of 14 (solid line), 12 (dotted line), 10 (dot-dash line), 8 (long dash line), and 6 (dot-long dash line) Gyr, as deduced from Bertelli et al. (1994) and Girardi et al. (1996). The arrows indicate the effect on mass determination of a 0.2 dex error in the assumed $[\text{Fe}/\text{H}]$.